In situ observation of atomic redistribution in alloying gold-silver nanorods

Jessi E S van Der Hoeven, Tom a J Welling, Tiago a G da Silva, Jeroen E van den Reijen, Camille La Fontaine, Xavier Carrier, Catherine Louis, Alfons van Blaaderen, Petra E de Jongh

In situ observation of atomic redistribution in alloying gold-silver nanorods

Jessi E.S. van der Hoeven,[†,‡] Tom A. J. Welling,[‡] Tiago A. G. da Silva,[¶] Jeroen E. van den Reijen,[†] Camille La Fontaine,[§] Xavier Carrier,[¶] Catherine Louis,[¶] Alfons van Blaaderen,[*,‡] and Petra E. de Jongh[*,†]

†*Inorganic Chemistry and Catalysis, Debye Institute for Nanomaterials Science, Utrecht University, Universiteitsweg 99, 3584 CG Utrecht, The Netherlands*

‡*Soft Condensed Matter, Debye Institute for Nanomaterials Science, Utrecht University, Princetonplein 5, 3584 CC Utrecht, The Netherlands*

¶*Sorbonne Université, CNRS, Laboratoire de Réactivité de Surface, LRS, F-75005, Paris, France*

§*Synchrotron SOLEIL, L'Orme des Merisiers, BP 48, Saint-Aubin, 91 192 Gif-sur-Yvette, France*

E-mail: A.vanBlaaderen@uu.nl; P.E.deJongh@uu.nl

Abstract

The catalytic performance and optical properties of bimetallic nanoparticles critically depend on the atomic distribution of the two metals in the nanoparticles. However, at elevated temperatures, during light induced heating or during catalysis atomic redistribution can occur. Measuring such metal redistribution *in situ* is challenging and a single experimental technique does not suffice. Furthermore, the availability of a well-defined nanoparticle system has been an obstacle for a systematic investigation of the key factors governing the atomic redistribution. In this study, we follow metal

redistribution in precisely tunable, single-crystalline Au-core Ag-shell nanorods *in situ*, both at a single particle and ensemble averaged level, by combining *in situ* TEM with *in situ* EXAFS validated by *ex situ* measurements. We show that the kinetics of atomic redistribution in Au-Ag nanoparticles depend on the metal composition and particle volume, where a higher Ag-content or a larger particle size lead to significantly slower metal redistribution. We developed a simple theoretical model based on Fick's first law which can correctly predict the composition and size dependent alloying behavior in Au-Ag nanoparticles as observed experimentally.

Keywords

alloying, bimetallics, *in situ* electron microscopy, *in situ* EXAFS, modelling

Introduction

By combining two metals in bimetallic nanoparticles (NPs) new and enhanced optical and catalytic properties can arise, which can lead to applications in e.g. sensing, biomedicine, data storage and catalysis[1–10]. The physicochemical properties of these bimetallic particles can not only be tuned by varying the metal composition, but also by changing the atomic distribution of the two metals within the nanoparticles at a fixed composition, for example from core-shell to alloyed NPs[8,10–15]. The exact atomic distribution of the metals is particularly important in catalysis where the atoms close to the surface play a dominant role in the catalytic performance[7,16–19]. Furthermore, when exposing bimetallic nanoparticles to various gas atmospheres and heating them to elevated temperatures atomic redistribution can occur[11,17,18,20–26]. This alters the optical[8,13,26] and catalytic properties[16–18,24,27], and can even lead to severe deactivation of the catalyst. Therefore, understanding atomic restructuring is crucial in the design of new catalytic and optical bimetallic materials.

Various techniques have been employed to follow metal redistribution *in situ*, each pro-

viding information on a different length scale[20]. Single-particle studies often make use of *in situ* Transmission Electron Microscopy (TEM). With this technique sub-nanometer or even atomic resolution can be obtained while heating the sample[17,21,22]. This technique, however, is limited to samples that are very stable under electron irradiation, in order to avoid electron beam induced artefacts[28–30]. Therefore, to verify the influence of the electron beam, it is important to also perform *ex situ* heating measurements[30]. Alternatively, X-ray based techniques, such as X-ray Photoelectron Spectroscopy (XPS) and X-ray Absorption Fine Structure (XAFS), also offer atomic information, but averaged over a much larger number of particles[18,25]. XPS allows to specifically study the surface composition of the NPs and it is thus particularly suitable to measure surface segregation effects[17,23,24]. On the other hand, XAFS measurements give insight in the degree of mixing and oxidation state of the atoms within the nanoparticles, and can be carried out in different gas atmospheres[14,18,25]. Thus, to follow the metal redistribution in bimetallic nanoparticles at multiple length scales - on an atomic, single-particle and ensemble-averaged level - one technique does not suffice and a multi-technique approach is required.

In addition, a systematic, quantitative and reproducible study of atomic restructuring requires a well-defined model system. The use of rather heterogeneous bimetallic catalysts, obtained via standard catalyst preparation methods, is especially problematic when using techniques like XAFS and XPS, where the measured signal is an ensemble average. Therefore, the influence of fundamental parameters such as the metal composition and particle volume on the atomic redistribution process in bimetallic nanoparticles are largely unexplored.

In this study, we investigated the thermally driven atomic redistribution in single crystalline Au-Ag core-shell nanorods *in situ* both on a single particle and ensemble averaged level. We employed colloidally synthesized Au-core Ag-shell nanorods of which the composition, size and shape was tuned precisely[9]. By coating the metal nanorods with a protective mesoporous silica coating[31], preservation of the particle shape during atomic redistribution was ensured[8]. We specifically chose a Au-Ag based system, since alloy formation is ther-

modynamically favourable at all compositions and the lattice spacings of Au and Ag closely match[32]. As the nanorods are single crystalline, this model system is well suited to specifically study the kinetics of metal redistribution during alloying. To this end, we performed both *in situ* TEM and *in situ* EXAFS measurements, yielding sub-nm, single particle and atomic, ensemble averaged information, respectively. In addition, we validated the *in situ* measurements with *ex situ*measurements carried out in the absence of an electron or X-ray beam. In particular, we addressed the influence of the metal composition (Au-Ag ratio) on the alloying temperature of the Au-core Ag-shell nanorods. We unambiguously showed the influence of the metal composition on the kinetics of the alloying process. An increasing Ag-content led to slower metal redistribution, a trend which is opposite to the dependence of the melting temperature on the Au-Ag ratio. We developed a simple theoretical model that correctly predicts the temperatures and time scales for metal redistribution as a function of particle volume and composition. Our study does not only demonstrate a general, multi-scale approach to monitor metal redistribution in bimetallic nanoparticles, but also reveals the influence of fundamental parameters governing metal redistribution which is of importance in bimetallic nanoparticles applications.

Results and Discussion

Preparation of core-shell nanorods

Mesoporous silica coated Au-core Ag-shell nanorods (Au@Ag@SiO_2 NRs) with similar volumes, but with 3 different Au-Ag ratios were colloidally synthesized. The colloidal synthesis was performed on a relatively large, milligram scale in order to obtain the required amount of sample needed for the EXAFS measurements. To this end, the Ag-shell growth as described by Deng *et al.*, comprising the reduction of Ag^+ ions on the Au nanorods by ascorbic acid, was performed in an acidified, instead of neutral, aqueous solution[9]. The presence of H^+ ions slowed the Ag-shell growth down considerably (from seconds to minutes), resulting in

sufficiently long mixing times for the reagents and homogeneous Ag-shell growth. To limit the variation in particle volume when changing the Au-Ag ratios of the particles, both the core and the shell size of the Au-core and Ag-shell were varied. In this way, 3 batches of mesoporous silica coated Au-core Ag-shell NRs with an average atomic Ag fraction X_{Ag} of 0.20, 0.46 and 0.70 and an average particle volume V of 2.2, 4.1 and 5.6·10^4 nm^3 were obtained, respectively. To also investigate the influence of the particle volume on the atomic redistribution, a batch of considerably smaller Au@Ag@SiO_2 NRs with average $X_{Ag} = 0.46$ and $V = 0.7{\cdot}10^4$ nm^3 was prepared.

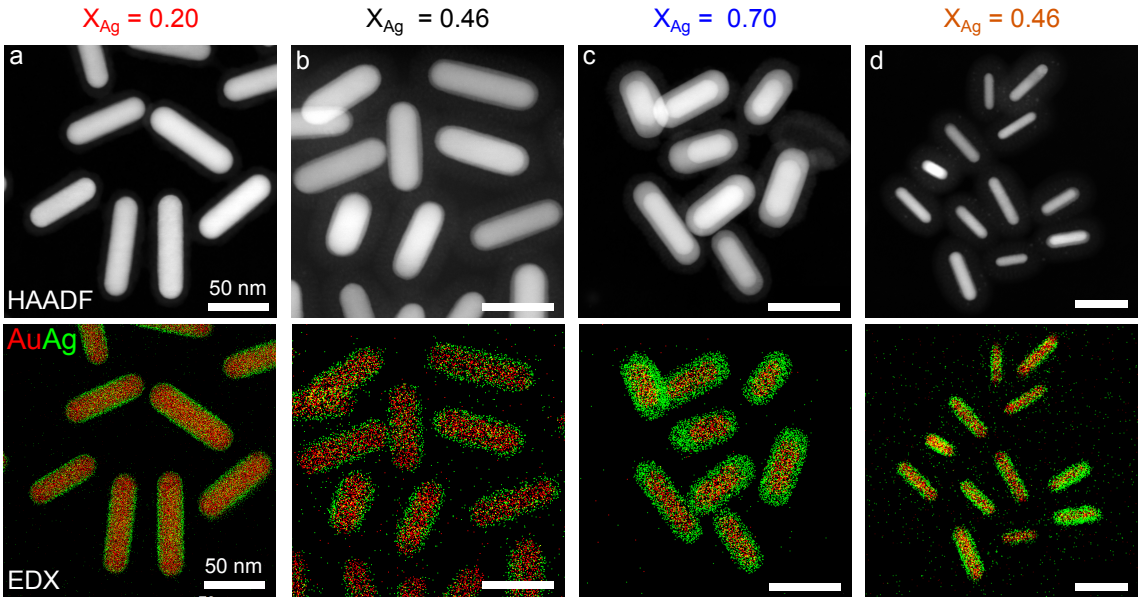

Figure 1: **Electron microscopy images of mesoporous silica coated Au-core Ag-shell nanorods (Au@Ag@SiO_2 NRs) with different X_{Ag} ratios and particle volumes.** Top: HAADF-STEM images. Bottom: EDX maps with Au and Ag in red and green, respectively. Au@Ag@SiO_2 NRs with $X_{Ag} = 0.20$; $V = 2.2{\cdot}10^4$ nm^3 (a, red), $X_{Ag} = 0.46$; $V = 4.1{\cdot}10^4$ nm^3 (b, black), $X_{Ag} = 0.70$; $V = 5.6{\cdot}10^4$ nm^3 (c, blue) and $X_{Ag} = 0.46$; $V = 0.7{\cdot}10^4$ nm^3 (d, orange). The Si signal is not shown in the EDX maps (see Figure S1).

In Table 1 we report a summary of the sample details and in Figure 1 we show the corresponding High Annular Dark-Field Scanning Transmission Electron Microscopy (HAADF-STEM) images and Energy Dispersive X-ray spectroscopy (EDX) maps. Due to the large Z-contrast difference between Au and Ag atoms, the core-shell structure of the nanorods is readily visible in the HAADF-STEM images. The different Ag-contents are most clearly

Table 1: **Sample details for the Au@Ag@SiO_2 NRs depicted in Figure 1**. The average and corresponding standard deviations of the atomic Ag fraction, length, diameter and volume are indicated with X_{Ag}, L, D and V, respectively. The values were based on 50 measurements per sample.

X_{Ag}	L (nm)	D (nm)	V ($\cdot 10^4$ nm^3)
0.20	67±10	21±2.1	2.2±0.58
0.46	74±8.7	28±1.9	4.1±0.77
0.70	80±9.2	32±3.8	5.6±1.6
0.46	48±9.2	14±1.8	0.7±0.3

seen in the EDX maps, where Au and Ag are depicted in red and green, respectively. The Si signal of the silica shell is shown in the SI (Figure S1) together with the optical spectra (Figure S2) and a high resolution TEM image showing the single crystalline structure of the nanorods (Figure S3).

Direct visualization of metal redistribution in individual particles with *in situ* TEM

In situ TEM was used to visualize the atomic redistribution in individual NRs with different Au-Ag ratios and volumes. To avoid variations between *in situ* TEM measurements on different samples due to e.g. inequalities in the heating temperature or differences in electron dose which are known to be important in *in situ* electron microscopy[28–30], we chose to compare 4 different samples in one measurement under exactly the same conditions. To achieve this, a mixture of the 4 samples with different Au-Ag ratios and particle volumes was deposited on a single SiN_x chip. The heating experiment was carried out in high vacuum with a ramp of 3 °C/min. EDX analysis was used to map the Au and Ag metal distribution as a function of temperature.

Figure 2a shows the EDX maps of the mixture of Au@Ag@SiO_2 NRs at various temperatures. The EDX maps of the orange, red, grey and blue highlighted NRs in Figure 2a are enlarged in Figure 2b. We determined the Ag-fractions and particle volumes of these individual nanorods, which were slightly different from the average values in Table 1: $X_{Ag} = 0.44$

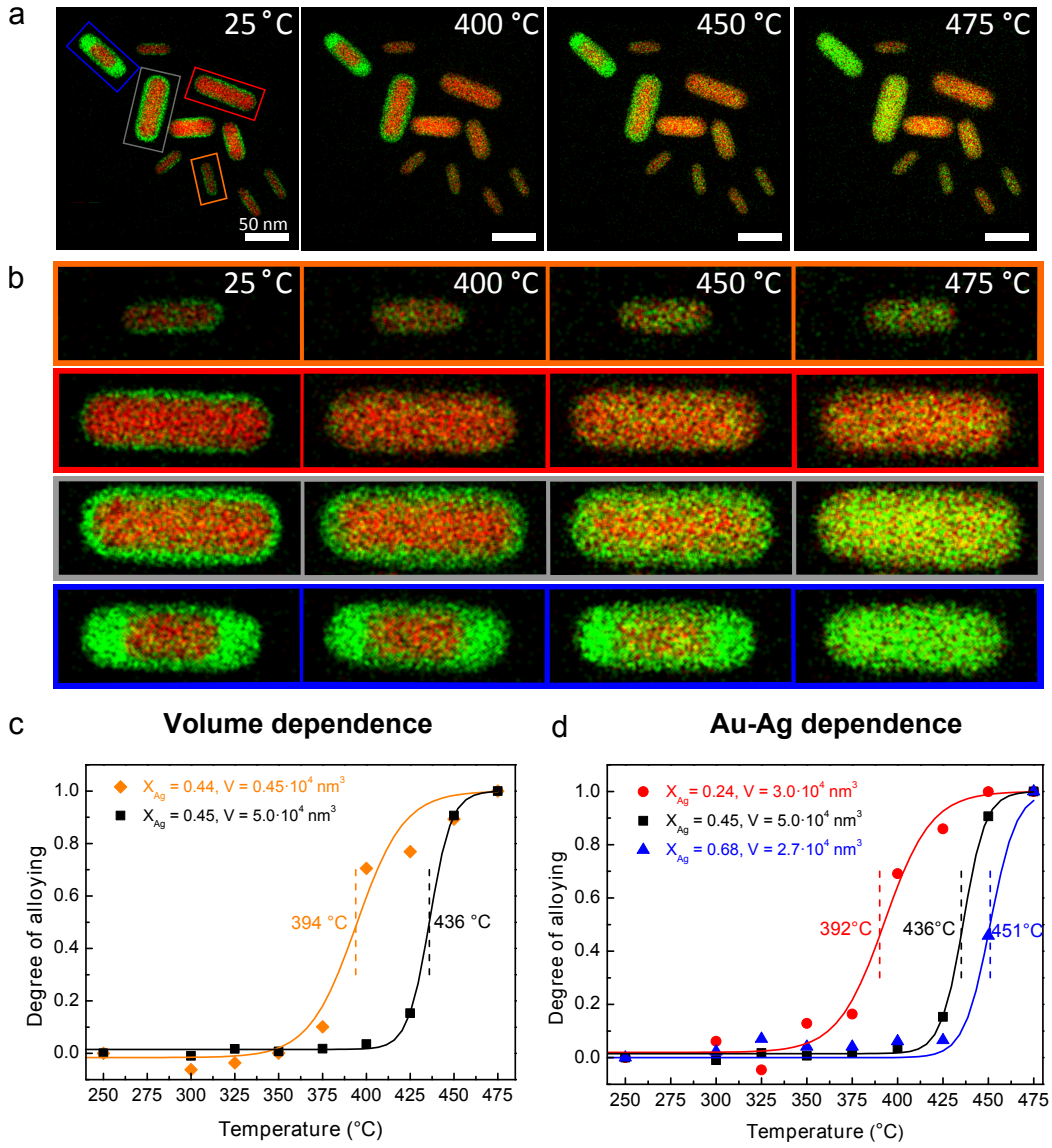

Figure 2: **Direct visualization of atomic redistribution in individual Au@Ag@SiO$_2$ NRs with in situ heating TEM.** (a, b) EDX maps acquired at 25, 400, 450 and 475 °C. (c) Particle volume dependence of the degree of alloying for Au@Ag@SiO$_2$ NRs with $V = 0.45{\cdot}10^4$ nm^3 ($X_{Ag} = 0.44$, orange) and $V = 5.0{\cdot}10^4$ nm^3 ($X_{Ag} = 0.45$, black). (d) The degree of alloying as a function of Ag-content with Au@Ag@SiO$_2$ NRs of $X_{Ag} = 0.24$ ($V = 3.0{\cdot}10^4$ nm^3, red), X_{Ag} 0.45 ($V = 5.0{\cdot}10^4$ nm^3, black) and $X_{Ag} = 0.68$ ($V = 2.7{\cdot}10^4$ nm^3, blue). Curves are best fit to the experimental data. The heating ramp was set to 3 °C/min.

$V = 0.45{\cdot}10^4$ nm^3 (orange), X_{Ag}= 0.45 $V = 5.0{\cdot}10^4$ nm^3 (black) $X_{Ag} = 0.24$ $V = 3.0{\cdot}10^4$ nm^3 (red) and $X_{Ag} = 0.68$ $V = 2.7{\cdot}10^4$ nm^3 (blue). To precisely track the metal redistribution in these individual nanorods during the heating process, we determined the core-to-shell ratio from the core and shell diameter for each particle at each temperature (see Figure S4 for

details on the analysis procedure). From the core-to-shell ratios we derived the degree of alloying at the different heating temperatures, which increases from 0 to 1 when going from a core-shell to an alloyed nanorod. In Figure 2c we plot the alloying curves of the black and orange highlighted single particles as a function of temperature for the 2 particles with the same Au-Ag ratio, but a factor 10 difference in particle volume. The plot in Figure 2d shows the individual alloying curves of the particles in red, black and blue, which have a similar volume but different Au-Ag ratios. We defined the alloying temperature T_{Alloy} as the temperature where the degree of alloying reached 0.5 and was 392, 394, 436 and 451 °C for the rods with $X_{Ag} = 0.24$, $X_{Ag} = 0.44$, $X_{Ag} = 0.45$ and $X_{Ag} = 0.68$, respectively.

These *in situ* TEM measurements clearly show the impact of the particle volume and the metal composition on the atomic redistribution, where an increase in particle volume and Ag-content led to significantly higher alloying temperatures. The difference in alloying temperature for the Au@Ag@SiO_2 NR with the lowest ($V = 0.45{\cdot}10^4\,nm^3$) and highest particle volume ($V = 5.0{\cdot}10^4\,nm^3$) was 42 °C. Although a factor 10 difference in particle volume led to a significant decrease in alloying temperature, the influence of the particle volume for the NRs of $V = 1.3$ to $3.0{\cdot}10^4\,nm^3$ was negligible (Figure S5), showing that only large differences in particle volume have a significant effect on the alloying temperature. From EDX maps and corresponding alloying curves in Figure 2b and d it is clear that the atomic redistribution is strongly influenced by the Au-Ag ratio: the Au@Ag@SiO_2 NR with the $X_{Ag} = 0.68$ alloyed at almost 50 °C higher than the one with $X_{Ag} = 0.24$. Despite the fact that the rod with $X_{Ag} = 0.68$ had a 2 times smaller volume than the rod with $X_{Ag} = 0.45$, the increase in Ag-content led to a significantly higher alloying temperature.

Ensemble averaged atomic redistribution from *in situ* EXAFS

To investigate the impact of the metal composition on the atomic redistribution for a larger number of particles, we moved from *in situ* TEM to *in situ* EXAFS and extended our study from a femtogram to milligram scale, and from single to 10^{19} particles. Additionally, *in*

situ EXAFS measurements allowed dosing of gases combined with a reliable temperature control. The unconventionally fast switching between the metal absorption edges ($< 1\,\text{min}$) at the ROCK beamline of the SOLEIL synchrotron made it possible to follow the atomic redistribution at the Au and Ag absorption edges in the same experiment. The alloying experiments were carried out under inert conditions in a He-flow, since the presence of oxygen is known to significantly change the alloying process[8].

The *in situ* EXAFS data of the atomic redistribution in the Au@Ag@SiO_2 NRs with lowest and highest Ag-content, $X_{Ag} = 0.20$ and 0.70 are shown in Figure 3. Figure 3a-d shows the normalized μ(E) spectra and χ(k) spectra acquired at the Au L_3 and Ag K absorption edges of the NRs with $X_{Ag} = 0.70$. The oxidation state of the Au and Ag atoms in the core and in the shell of the NRs before heating was determined from the XAFS spectra at room temperature (RT) and found to be predominately metallic (Figure S6). The *in situ* EXAFS spectra show a clear change when heating the NRs from 30 to 500 °C. To verify if metal redistribution took place, we used the EXAFS spectra before and after thermal treatment to calculate the coordination numbers between the Au and Ag atoms: N_{Au-Au}, N_{Au-Ag}, N_{Ag-Ag} and N_{Ag-Au}. Table 2 lists the coordination numbers for both samples. Due to the core-shell structure of the NRs the coordination numbers between unlike atoms are low before heating. As expected, N_{Ag-Au} is lowest for core-shell particles with the highest X_{Ag}. After heating the core-shell NRs to 500 °C, N_{Ag-Au} and N_{Au-Ag} increased by a factor ≥ 6, indicating that mixing of the two elements took place in both samples. A full overview of the EXAFS fitting parameters is given in Table S1-S4.

To estimate if the NRs were fully alloyed, meaning that the Au and Ag atoms were randomly dispersed within the particles, the extent of alloying (J) was calculated following the approach developed by Hwang *et al.*[14]:

$$J_{Au} = \frac{P_{observed}}{P_{random}} = \frac{[N_{Au-Ag}/(N_{Au-Ag} + N_{Au-Au})]_{observed}}{[N_{Au-Ag}/(N_{Au-Ag} + N_{Au-Au})]_{random}} \times 100\% \quad (1)$$

The J-values of the two components (Au and Ag) give information on the internal dis-

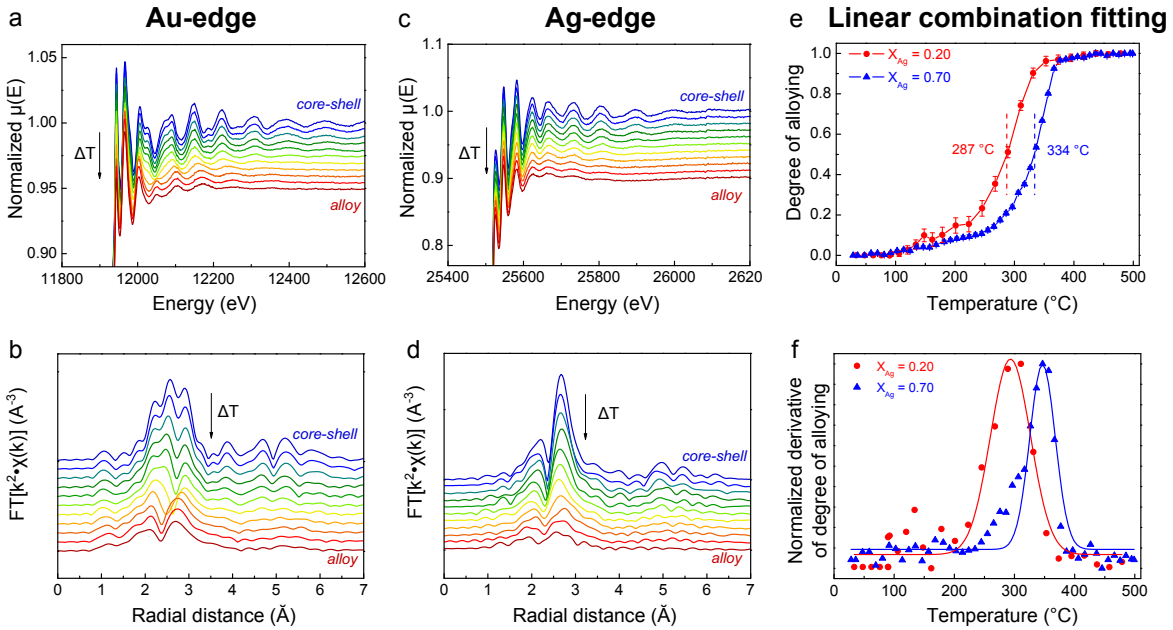

Figure 3: **Double edge *in situ* EXAFS measurements of Au@Ag@SiO_2 NRs upon heating.** Normalized $\mu(E)$-spectra and FT$[k^2\chi(k)]$ spectra at the Au L_3-edge (a,b, Δk = 3.3-14.0 Å^{-1}) and Ag K-edge (c,d, Δk = 3.2-12.0 Å^{-1}) of the nanorods with $X_{Ag} = 0.70$, recorded every ∼50 °C when heating from 30 to 500 °C. The plots in e and f show the degree of alloying and the derivative thereof as a function of temperature and were obtained by performing linear combination fitting on the normalized $\mu(E)$-spectra at the Ag K-edge ($X_{Ag} = 0.20$, red) and Au L_3-edge ($X_{Ag} = 0.70$, blue). The EXAFS spectra were acquired during heating to 500 °C with 3 °C/min in a 25 mL/min He-flow.

Table 2: **Coordination number N before and after heating the NRs to 500 °C** in a 25 mL/min He-flow with a 3 °C/min ramp. Based on the coordination numbers the corresponding J-values were calculated.

	N_{Ag-Ag}	N_{Ag-Au}	N_{Au-Au}	N_{Au-Ag}	J_{Ag}	J_{Au}
$X_{Ag} = 0.20$ before heating	10.1±1.8	1.1±1.3	11.0±0.2	0.3±0.2	12	13
$X_{Ag} = 0.20$ after heating	2.5±0.7	6.8±1.7	9.6±0.2	1.8±0.1	91	79
$X_{Ag} = 0.70$ before heating	11.0±0.3	0.6±0.3	9.8±0.2	0.3±0.2	17	4
$X_{Ag} = 0.70$ after heating	7.7±0.4	3.5±0.2	3.1±0.3	8.3±0.4	104	104

tribution of the two components[14]. To calculate P_{random} the Au-Ag ratios as determined by EDX were used. In table 2 the J-values for the two different NR samples before and after heating to 500 °C are given. For both alloyed samples the calculated J_{Au} and J_{Ag}-values are close to 100, indicating that the NRs are likely to have a fully alloyed structure when

heating them to 500 °C.

To deduce the evolution of the alloying process from all the spectra acquired between 30 and 500 °C, we performed linear combination fitting on the normalized μ(E) spectra. In (E)XAFS analysis, linear combination fitting is typically used to determine and/or follow changes in the oxidation state of metal nanoparticles, but not common for following metal redistribution. Note that a linear combination fitting based analysis is considerably faster than calculation of the coordination numbers, which is especially important when analysing a large number of EXAFS spectra.

In our analysis, each EXAFS spectrum at a given temperature was compared to the spectrum of the initial core-shell and final alloyed state for which the spectra at 30 °C and 500 °C were taken, respectively. As shown in Figure 3e, the analysis was successfully applied to obtain the degree of alloying as a function of temperature. Figure 3e specifically shows the linear combination fitting results determined from the Ag K-edge for the $X_{Ag} = 0.20$ sample and Au L_3-edge for the $X_{Ag} = 0.70$ sample, since the change from core-shell to alloyed state is most apparent on the edge of the least abundant metal. In addition, it is important to note that the linear combination fitting analysis is also sensitive to changes which are not due to metal redistribution, such as damping of the EXAFS spectra due to thermal disorder with increasing temperature. This temperature contribution predominately plays a role when the change upon alloying is small, as is the case for the absorption edge of the metal which is in the majority (Figure S7 and S8).

From Figure 3e the alloying temperature determined at a degree of alloying of 0.5, was 287 and 334 °C for the sample with $X_{Ag} = 0.20$ and 0.70, respectively. The EXAFS measurements thus confirmed the increase in alloying temperature with increasing Ag-content as observed in the *in situ* TEM, but now for a large ensemble of particles. However, it should be noted that there is a discrepancy in alloying temperatures: from the *in situ* EXAFS we obtained ∼100 °C lower alloying temperatures compared to the *in situ* TEM data. This discrepancy demonstrates the need for *ex situ* measurements to establish the absolute temperature at

which the metal redistribution occurs in the absence of an electron or X-ray beam.

Validation of the *in situ* data

Although electron microscopy and X-ray absorption spectroscopy enable the *in situ* observation of structural changes in metal nanoparticles, it is crucial to validate these techniques with *ex situ* measurements. In particular electron beam irradiation has been reported to induce anomalous behavior in nanostructured materials and significantly alter the deformation behavior, growth kinetics and structure of the nanoparticles during *in situ* studies[28–30]. To verify the dependence of the alloying temperature on the Au-Ag ratio as observed in *in situ* TEM and *in situ* EXAFS, *ex situ* measurements were carried out, heating the NRs in a furnace. Herein, we used the same heating ramp of 3 °C/min to heat to 250, 300, 325, 350, 375 and 400 °C in N_2 after which each sample was analysed with HAADF-STEM and EDX (Figure S9). In every sample and for each temperature, 4 representative rods were analysed with EDX to determine their core-to-shell ratios and their compositions, which were close to the average sample compositions as given in Table 1. From the core-to-shell ratio the degree of alloying was calculated in the same way as described for the *in situ* TEM measurements and the degree of alloying is shown as a function of the heating temperature in Figure 4a. It shows that the Au@Ag@SiO_2 NRs with average $X_{Ag} = 0.17$, 0.46 and 0.72 alloy at 305, 345 and 375 °C, respectively. The EDX maps in Figure S9 show that all Au@Ag@SiO_2 NRs of the same composition simultaneously convert from a core-shell to alloyed state.

In Figure 4b an overview of the alloying temperatures versus the Ag-content for all three techniques is shown. The *ex situ* data nicely support the trends observed in the *in situ* TEM and *in situ* EXAFS measurements. In all three techniques the alloying temperature increases with an increasing Ag-content, only the absolute temperatures vary. The *ex situ* TEM measurements match the EXAFS results, but the alloying temperatures determined by *in situ* TEM are 75-90 °C too high. The relatively high alloying temperatures from the *in situ* TEM measurements could be related to an altered heat conductivity in the SiN_X chip

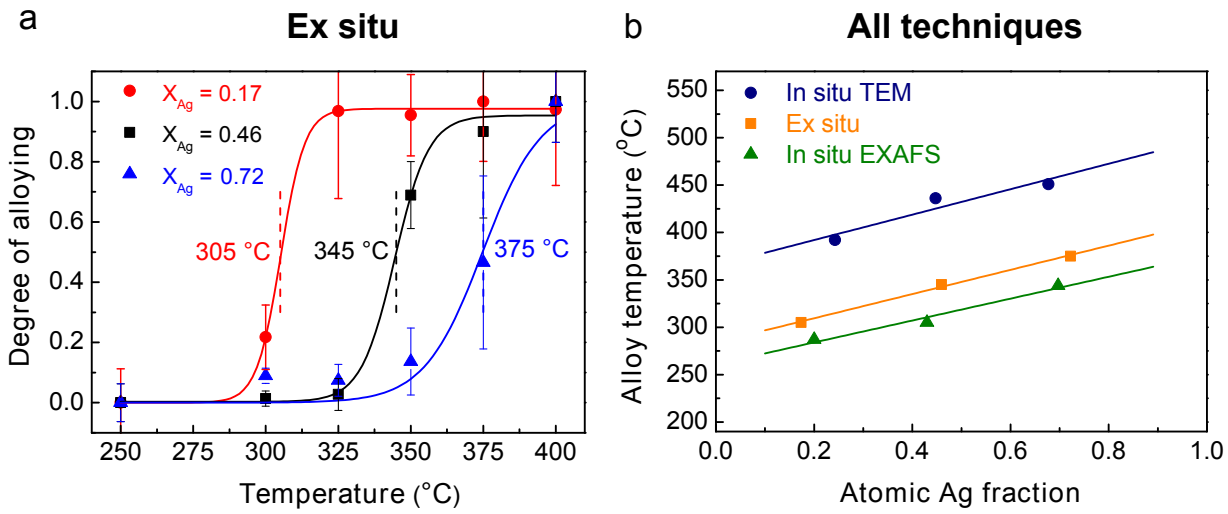

Figure 4: ***Ex situ* TEM measurements on the alloying of Au@Ag@SiO_2 NRs.** a) the degree of alloying after heating Au@Ag@SiO_2 NRs in a furnace as a function of the heating temperature. Each point is an average of 4 particles. The alloying temperatures for the Au@Ag@SiO_2 NRs with $X_{Ag} = 0.17$ (red), 0.46 (black) and 0.72 (blue) was 305, 345 and 375 °C, respectively. The samples were heated in a N_2 flow with a heating ramp of 3 °C/min. b) summary of the alloying temperature as a function of Ag fraction determined with *in situ* TEM (dark blue), *ex situ* TEM (orange) and *in situ* EXAFS (green). Curves are best fit to the experimental data.

after depositing the nanorods combined with possible carbon contamination, leading to inaccurate temperatures in the heating chip. Alternatively, the strongly reducing electron beam could have influenced the kinetics of the alloying process, but we did not observe significant differences in the alloying process between areas that were or were not not illuminated with the electron beam prior to the heating. Thus, although care should be taken in deducing quantitative data from *in situ* TEM, it is a powerful technique in providing a qualitative insight in the metal redistribution for single nanoparticles and correctly shows the dependency of the metal redistribution on the metal composition for different nanoparticles.

It should be noted that the observed trend between the diffusion and metal composition in the Au-Ag nanoparticles varies oppositely to the melting temperature, which is 962 for Ag and 1064 °C for Au. A similar trend for atomic diffusion was measured in bulk Au-Ag crystals[33]. The activation energy of diffusion for both Au and Ag atoms in Au-Ag alloys was reported to increase with increasing Ag fraction going from 1.74 to

1.93 eV for Ag atoms in pure Au and Ag, and 1.81 to 2.09 eV for Au atoms in pure Au and Ag[33]. From these activation energies it follows that Ag atoms are more mobile than Au atoms, but that the diffusion of both Au and Ag atoms is slower in high Ag-content Au-Ag alloys. A possible explanation for this phenomenon can be derived from the energy of vacancy formation and atom migration, which are known to be higher in Ag compared to Au: E(vacancy formation)$_{Ag}$= 1.10 eV, E(vacancy formation)$_{Au}$= 0.97 eV, E(atom migration)$_{Ag(in)Ag}$= 0.83 eV, E(atom migration)$_{Ag(in)Au}$= 0.77 eV[33–35]. Since atomic diffusion in Au-Ag crystals is known to go via vacancy hopping, a lower number of vacancies and a higher energy cost for hopping into the vacancies with increasing Ag-content could explain the observed retardation of Au and Ag in high content Ag alloys. In addition to Au-Ag, similar trends of self-diffusion dependency opposite to melting temperature have been reported for e.g. Ag-Mn[36], TiCr[37,38] and Tl-Pb bulk crystals[39]. In this study, we show the first observation of this trend at the nanoscale.

Modelling atomic redistribution

We devised a simple model that can correctly describe the diffusion in Au-Ag nanoparticles as a function of temperature and composition. We numerically calculate the diffusion of Au atoms n_{Au} and Ag atoms n_{Ag} passing through a static Au-Ag interface per time step Δt according to Fick's first law:

$$n_{Ag}/\Delta t = (A/r) \cdot D_0^{Ag} e^{-Q_{Ag}/(RT)} \cdot |C_{core}^{Ag} - C_{shell}^{Ag}| \tag{2}$$

where A is the interface area, r the radius of the NP, D_0^{Ag} the frequency factor, Q_{Ag} the activation energy, R the gas constant, T the temperature, C_{core}^{Ag} the silver concentration of the core and C_{shell}^{Ag} the silver concentration of the shell (expressed in atoms per m^3). An analogous formula holds for the Au atoms. The rate of diffusion was calculated iteratively, where D_0, Q and the concentration difference $C_{core} - C_{shell}$ were updated every time step. The frequency

factor D_0 and activation energy for diffusion Q depend on the Au-Ag composition and have been measured experimentally in bulk crystals[33]. We corrected these composition dependent bulk D_0 and Q values for the NP size according to the model of Guisbiers *et al.*[40,41]. Herein, the activation energy of diffusion in NPs Q_{NP} was derived from the activation energy of diffusion in the bulk Q_{Bulk} by using a so-called shape factor α_{shape} which amongst others depends on the surface-to-volume ratio of the NPs. More details on the calculation of the α_{shape} factor can be found in the experimental section. For the Au-Ag NRs used in this study, the correction of Q_{Bulk} to Q_{NP}, resulted in alloy temperatures of ~50 °C lower compared to bulk crystals of the same Au-Ag composition.

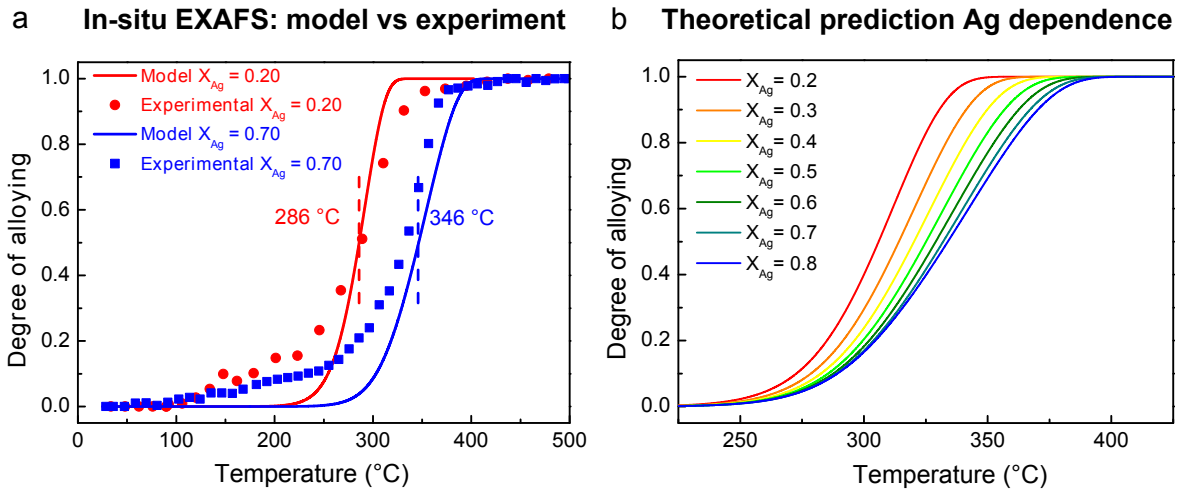

Figure 5: **Theoretical prediction of the change in the degree of alloying as a function of heating temperature and atomic Ag fraction.** (a) The theoretical prediction for the *in situ* EXAFS experiment give an alloying temperature of 286 and 346 °C for the samples with $X_{Ag} = 0.20$ and 0.70. The plot in b shows the theoretical prediction of the alloying curves for Au-Ag NRs of $V = 4{\cdot}10^4$ nm^3 and $X_{Ag} = 0.2$-0.8 (red-blue) heated with 3 °C/min.

The resulting theoretical predictions for the alloying curves of the *in situ* EXAFS measurements are shown in Figure 5a. The theoretical predictions are in very good agreement with the experimental *in situ* EXAFS data and the alloying temperatures as predicted by the model, 286 and 346 °C for the $X_{Ag} = 0.20$ and 0.70, match the experimental values of 287 and 334 °C closely. In Figure 5b we show the theoretical prediction for the alloying curves

of Au-Ag NRs with $V = 4{\cdot}10^4$ nm^3 and $X_{Ag} = 0.2$-0.8. In the calculation of these curves a heating ramp of 3 °C/min was considered, as in the experimental studies. The inset in Figure 5b displays the alloy temperature as a function of the Ag-fraction. The theoretical predictions clearly demonstrate the importance of including the dependency of the diffusion on the metal composition. We would like to stress that it is remarkable that the metal composition still plays such a crucial role in the diffusion kinetics in nanoparticles, where size and shape have generally been considered to play the most important role[12,32,40] and the influence of the particle composition has therefore been neglected so far.

Conclusions

We have used a multi-technique approach to precisely follow metal redistribution, a process crucial in catalysis, *in situ* and at different length scales. A combination of *in situ* TEM with *in situ* EXAFS validated with *ex situ* measurements, provided both a single particle and ensemble averaged characterization. Our well-defined model system, consisting of mesoporous silica coated, single crystalline Au-core Ag-shell nanorods of tunable size and composition, allowed a systematic study of the nanoparticle composition on the atomic redistribution kinetics. We unambiguously showed that the atomic diffusion in Au-Ag nanoparticles strongly depends on the composition, a trend which has been observed in bulk crystals, but which has, to the best of our knowledge, not been reported for nanomaterials. Finally, we show that to correctly model metal redistribution in metallic nanoparticles not only the nanoscale dimensions, but also the metal composition should be taken into account. Both our experimental approach and theoretical model are likely to apply to a wide range of bimetallic nanoparticle based materials.

Experimental

Chemicals

All chemicals were used as received without further purification. Hexadecyltrimethylammonium bromide (CTAB, >98.0%) and sodium oleate (NaOL, >97.0%) were purchased from TCI America. Hydrogen tetrachloroaurate trihydrate ($HAuCl_4$ H_2O) and sodium hydroxide (98%) were purchased from Acros Organics. L-Ascorbic Acid (BioXtra, ≥99%), silver nitrate ($AgNO_3$,≥99%), sodium borohydride ($NaBH_4$, 99%), hydrochloric acid (HCl, 37 wt% in water), tetraethyl orthosilicate (TEOS, 98%) and ammonium hydroxide solution (≥25 wt% in water) were purchased from Sigma-Aldrich. Ultrapure water (Millipore Milli-Q grade) with a resistivity of 18.2 MΩ was used in all of the experiments. All glassware for the AuNR synthesis was cleaned with fresh aqua regia (HCl/HNO_3 in a 3:1 volume ratio), rinsed with large amounts of water and dried at 100 °C before usage.

Synthesis of the Au-Ag nanorods

Three batches of $Au@Ag@SiO_2$ NRs with average Ag atomic fractions of 0.20, 0.46 and 0.70 were prepared by changing both the Au core size and the Ag-shell thickness. The synthesis of the AuAg core-shell rods consists of 4 steps: AuNR synthesis (I), mesoporous silica coating (II), partial etching of AuNRs within their mesoporous silica shells (III) and Ag-shell growth on the etched AuNRs (IV).

In the first step, monodisperse AuNRs were synthesized according to the protocol of Ye *et al.*[42]. Two 500 mL scale syntheses were carried out with growth solutions containing 7.0 g CTAB, 1.24 g NaOL, 25 mL MQ H_2O and 250 mL 1.0 mM $HAuCl_4$, 7.2 mL $AgNO_3$, 2.1 mL concentrated HCl, 64 mM ascorbic acid and 1.0 mL seed solution. The seeds were prepared from a 10 mL 0.10 M CTAB, 51 μL $HAuCl_4$ and 1.0 mL $NaBH_4$. The subsequent rod growth was performed under static conditions in a 30 °C water bath overnight. The resulting AuNR suspensions had an absorption maximum of 4.0 at λ(LSPR)= 866 and 853 nm. The rods

were centrifuged at 8000 rcf for 30 min (Rotina 380R Hettich centrifuge), washed with H_2O and redispersed in 5.0 mM CTAB H_2O.

In the second step, the CTAB stabilized AuNRs were coated with a 18 nm mesoporous silica shell via the method of Gorelikov *et al.*[31]. The coating was performed in 350 mL 1.5 mM CTAB aqueous solution containing 1.0 mM NaOH and an AuNR concentration corresponding to a absorption maximum of 10. While magnetically stirring at 300 rpm in a 30 °C waterbath, 3 times 1.05 mL 20 vol% TEOS in EtOH were added with a 30 min time interval. The Au@SiO_2 NRs were centrifuged at 8000 rcf for 30 min, washed with water and ethanol.

The third step, oxidative etching of the Au@SiO_2 NRs, was performed by following the procedure described by Deng *et al.*[9], but with H_2O_2 as an oxidant instead of O_2 from air. Different core sizes were obtained by varying the etching time. For the rods with $X_{Ag} = 0.20$ 240 mL AuNRs in MeOH (Abs = 6.0) were heated to 60 °C in an oil bath while magnetically stirring at 400 rpm. 4.8 mL HCl (37 %) and 4.8 mL H_2O_2 (0.2 wt%). The LSPR peak position changed from 838 nm to 822 nm after etching for 10 minutes. The reaction was quenched by putting the mixture in a 4 °C waterbath and diluting it with 200 mL icecold MeOH before centrifugation at 10000 rcf for 20 min. The etched rods were washed with and redispersed in EtOH. For batches with $X_{Ag} = 0.46$ and $X_{Ag} = 0.70$ 210 mL AuNRs in MeOH 4.8 mL HCl (37 %) and 4.8 mL H_2O_2 (0.2 wt%) were added. After 13 and 26 minutes, 100 mL reaction mixture was quenched with 100 mL icecold MeOH and was as described above. The LSPR peak postion of the rods were 750 nm and 694 nm.

Finally, the procedure by Deng *et al.* was modified to do the Ag-overgrowth in large reaction volumes ($\gg$ 1 mL). HCl was added to lower the Ag reduction rate by ascorbic acid and allows for a homogeneous shell growth on all particles. The rods with $X_{Ag} = 0.20$ were prepared by adding 2.0 mL 0.1 M HCl, 3.0 mL 5.0 mM $AgNO_3$ and 3.0 mL 20 mM ascorbic acid were added to 200 mL aqueous AuNR suspension (Abs = 4.5, LSPR = 780nm)

while stirring vigorously. The rods with $X_{Ag} = 0.70$ were prepared in 2 steps. To 120 mL rod suspension, 1.2 mL 0.1 M HCl, 6.6 mL 5.0 mM $AgNO_3$, 6.6 mL 20 mM ascorbic acid. After washing with MQ H_2O a second Ag-overgrowth step was performed to increase the Ag-content. To 100 mL aqeous Au@Ag@SiO_2 NRs suspension (Abs = 1.2 , LSPR = 701 nm), 1.0 mL 0.1 M HCl, 4.0 mL 5.0 mM $AgNO_3$ and 4.0 mL 20 mM ascorbic acid were added. The $X_{Ag} = 0.46$ sample was prepared on a smaller scale since it was only used for the *ex situ* and *in situ* TEM measurements. To 1.0 mL aqeous Au@SiO_2 NRs suspension (Abs = 2.5, LSPR = 745 nm), 10 μL 0.1 M HCl, 40 μL 5.0 mM $AgNO_3$, 40 μL 20 mM ascorbic acid were added.

All Au@Ag@SiO_2 NRs were washed with MQ H_2O, ethanol, redispersed in EtOH and stored at 4 °C to prevent oxidation and dissolution of the Ag-shell. The centrifugation speed varied between 6000 and 8000 rcf depending on the volume of the rods. The samples were dried at 60 °C in air. All samples were characterized with VIS-NIR spectroscopy and TEM.

In situ TEM

The *in situ* heating measurements were carried out on a FEI Talos F200X operated at 200 kV using a heating holder from DENSsolutions. A mix of 4 different batches of Au@Ag@SiO_2 NRs was dropcasted on a heating chip (Wildfire Nano-chip) with silicon nitride windows. The overall heating ramp was set to 3 °C/min. EDX maps were acquired at 25, 250, 300, 350 and from 400 to 650 °C with a 25 °C temperature interval. The acquisition time per EDX map was 5 min and the probe current 700 pA. In the intervals between the EDX acquisitions the beam was blanked to minimize the influence of the electron beam on the alloying process. Different SiN windows were checked during heating that where not illuminated prior to heating. No significant differences in alloying kinetics were observed between the illuminated and non-illuminated spots. The SiN chip was plasma cleaned for 10 s in a 20 % O_2 in Ar atmosphere before the TEM experiment.

In situ EXAFS

The *in situ* EXAFS measurements were performed at the ROCK beamline of the SOLEIL synchrotron. At this beamline, continuous switching between the Au L_3-edge (11919 eV) and the Ag K-edge (25514 eV) is possible (time to switch ∼1 min) using two Quick-XAS monochromators equipped with Si(111) and Si(220) channel-cut crystals, respectively. The operation parameters of the monochromators were set to record two EXAFS spectra per second. The powdered samples were loaded in a stainless steel sample holder (with a depth of 1 mm) allowing temperature control and gas flow. The X_{Ag} = 0.20 and X_{Ag} = 0.70 Au@Ag@SiO_2 NRs samples were diluted with boron nitride. The heating was done in a He flow of 25 mL/min and with a heating rate of 3 °C/min. Before and after heating, EXAFS spectra were collected for 500 s at each edge at RT and averaged. During the temperature ramps, alternate measurements at both edges were performed continuously: spectra were collected and averaged for 35 s at the Au edge and 60 to 120 s at the Ag edge, depending on the quality of the Ag-signal. Measurements were done in transmission mode, using ionization chambers as detectors. Energy calibration was ensured by the simultaneous measurement of the absorption spectra of metallic Au and Ag foils.

Spectra analysis was conducted with the IFEFFIT library using the GUI Athena and Artemis[43]. All spectra were energy calibrated to the first inflection point of the Ag or Au foil at 25514 eV and 11919 eV respectively. EXAFS signal was extracted in Athena with a R = 1.0 cut-off and k weight = 2 and Fourier transformed using a Hanning window in k = 3 and dk = 1. EXAFS analysis was conducted in Artemis with the normalized spectra exported from Athena. The amplitude reduction factor (S_0^2) of 0.83 for Ag and 0.79 for Au was obtained by fitting the EXAFS data of the respective metal foils. The simulation of scattering paths for the bimetallic samples was performed with the ATOMS algorithm with a custom input file created by substituting Au atoms by Ag in the first shell, to obtain the closest rational fraction of atoms. A correction factor was introduced to S_0^2 to obtain the actual sample composition. Structural parameters were determined by multiple k-weight

least-square fitting and the goodness of fit was determined by observing the reduced χ^2 and R^2 statistical parameters.

The linear combination fitting was carried out in Athena on the normalized $\mu(E)$-spectra in the region between -20 eV to 120 eV from the absorption edge.

Ex situ heating

The *ex situ* heating experiments were performed in a tubular oven (Thermolyne 79300 tube furnace) under a constant N_2 flow. The three different samples were each dropcasted on a copper TEM grid (200 mesh copper (100), Formvar/carbon film) and heated in a ceramic cup placed in a quartz oven tube. The heating rate was always 3 °C/min and the particles were heated to 250, 300, 325, 350, 375 and 400 °C and cooled down under N_2 to RT before taking them out of the oven. After heating all samples were analysed with HAADF and EDX on a FEI Talos F200X, operated under the same conditions as described above.

Diffusion model

To predict the rate of alloying in Au-Ag nanoparticles, we numerically calculated Fick's first law. The number of Au n_{Au} and Ag atoms n_{Ag} diffusing through the static Au-Ag interface per time step was calculated with equation 2. After each step the Au-Ag ratio of the core and the shell was updated, affecting D_0, Q, C_{core} and C_{shell} in Equation 2. The values for D_0 and Q for silver and gold diffusing into various Au-Ag compositions were taken from the work of Mallard *et al.*[33]. These bulk values of D_0 and Q were corrected for NP size effects according to the model of Guisbiers[40,41], in which the change in activation energy for a NP compared to the activation energy in the bulk can be described as

$$\frac{Q_{NP}}{Q_{bulk}} = 1 - \frac{\alpha_{shape}}{D} \tag{3}$$

where the shape factor α_{shape} is given by[40]

$$\alpha_{shape} = \frac{D(\gamma_s - \gamma_l)}{\Delta H_{m,\infty}} \times \frac{S}{V} \tag{4}$$

Here, D is the diameter of the NP, $\gamma_{s,l}$ are the surface energies in the solid and liquid phase, respectively, S the surface area of the NP, V the volume of the NP and $\Delta H_{m,\infty}$ the bulk melting enthalpy.

Lastly, the temperature was updated every time step according to the temperature ramp used in the experiments. Usually one time step was one second, which ensured small changes in the Au-Ag content per time step for the temperatures used in this work. Subsequent time steps were evaluated until the core and shell consist of the same Au-Ag composition, when a full alloy composition is reached. Only geometric input parameters determined from TEM such as the core-shell volume, the interface and surface area and the radius of the NP were needed for the calculations.

Acknowledgement

The authors thank Dr. M.A. van Huis for providing the *in situ* electron microscopy heating equipment, M. Bransen for useful discussion on the nanorod synthesis and Dr. S. Dussi for critically reading the manuscript. This project has received funding from the European Research Council (ERC) under the European Union's Horizon 2020 research and innovation programme (ERC-2014-CoG No 648991) and the ERC under the European Unions Seventh Framework Programme (FP-2007-2013)/ERC Advanced Grant Agreement #291667 HierarSACol. J.v.d.H. also acknowledges the Graduate programme of the Debye Institute for Nanomaterials Science (Utrecht University), which is facilitated by the grant 022.004.016 of the NWO, the Netherlands Organisation for Scientific research. The authors wish to acknowledge the award of beamtime on the ROCK beamline at Synchrotron SOLEIL under proposal number 20151175. The work on ROCK beamline was supported by a public grant

overseen by the French National Research Agency (ANR) as a part of the "Investissements d'Avenir" program (ref: ANR-10-EQPX-45).

References

(1) Gilroy, K. D.; Ruditskiy, A.; Peng, H.-C.; Qin, D.; Xia, Y. *Chem. Rev.* **2016**, *116*, 10414–10472.

(2) Dorleta Jimenez, d. A.; Ana Belén, S.-M.; Luis M., L.-M. *Adv. Opt. Mater.* **2015**, *3*, 602–617.

(3) Ferrando, R.; Jellinek, J.; Johnston, R. L. *Chem. Rev.* **2008**, *108*, 845–910.

(4) Singh, A. K.; Xu, Q. *Chem. Cat. Chem.* **2013**, *5*, 652–676.

(5) Liu, X.; Wang, A.; Yang, X.; Zhang, T.; Mou, C. Y.; Su, D. S.; Li, J. *Chem. Mater.* **2009**, *21*, 410–418.

(6) Sun, K. Q.; Hong, Y. C.; Zhang, G. R.; Xu, B. G. *ACS Catalysis* 1336–1346.

(7) Hong, J. W.; Kim, D.; Lee, Y. W.; Kim, M.; Kang, S. W.; Han, S. W. *Ang. Chem. Int. Ed.* **2011**, *50*, 8876–8880.

(8) Albrecht, W.; Van Der Hoeven, J. E. S.; Deng, T. S.; De Jongh, P. E.; Van Blaaderen, A. *Nanoscale* **2017**, *9*, 2845–2851.

(9) Deng, T. S.; Van Der Hoeven, J. E. S.; Yalcin, A. O.; Zandbergen, H. W.; Van Huis, M. A.; Van Blaaderen, A. *Chem. Mater.* **2015**, *27*, 7196–7230.

(10) Gao, C.; Hu, Y.; Wang, M.; Chi, M.; Yin, Y. *J. Am. Chem. Soc.* **2014**, *136*, 7474–7479.

(11) Bonifacio, C. S.; Carenco, S.; Wu, C. H.; House, S. D.; Bluhm, H.; Yang, J. C. *Chem. Mater.* **2015**, *27*, 6960–6968.

(12) Lasserus, M.; Schnedlitz, M.; Knez, D.; Messner, R.; Schiffmann, A.; Lackner, F.; Hauser, A. W.; Hofer, F.; Ernst, W. E. *Nanoscale* **2018**, *10*, 2017–2024.

(13) Pramanik, S.; Chattopadhyay, S.; Das, J. K.; Manju, U.; De, G. *J. Mater. Chem. C* **2016**, *4*, 3571–3580.

(14) Hwang, B. J.; Sarma, L. S.; Chen, J. M.; Chen, C. H.; Shih, S. C.; Wang, G. R.; Liu, D. G.; Lee, J. F.; Tang, M. T. *J. Am. Chem. Soc.* **2005**, *127*, 11140–11145.

(15) Ding, Y.; Fan, F.; Tian, Z.; Wang, Z. *J. Am. Chem. Soc.* **2010**, *132*, 12480–12486.

(16) Masoud, N.; Delannoy, L.; Calers, C.; Gallet, J. J. *Chem. Cat. Chem.* **2017**, *9*, 2418–2425.

(17) Zugic, B.; Wang, L.; Heine, C.; Zakharov, D. N.; Lechner, B. A. J.; Stach, E. A.; Biener, J.; Salmeron, M.; Madix, R. J.; Friend, C. M. *Nat. Mater.* **2016**, *16*, 558–565.

(18) Destro, P.; Kokumai, T. M.; Scarpellini, A.; Pasquale, L.; Manna, L.; Colombo, M.; Zanchet, D. *ACS Catal.* **2018**, *8*, 1031–1037.

(19) Sandoval, A.; Aguilar, A.; Louis, C.; Traverse, A.; Zanella, R. *J. Catal.* **2011**, *281*, 40–49.

(20) Tao, F.; Salmeron, M. *Science* **2011**, *331*, 171–174.

(21) Xin, H. L.; Alayoglu, S.; Tao, R.; Genc, A.; Wang, C. M.; Kovarik, L.; Stach, E. A.; Wang, L. W.; Salmeron, M.; Somorjai, G. A.; Zheng, H. *Nano Lett.* **2014**, *14*, 3203–3207.

(22) Holse, C.; Elkjær, C. F.; Nierhoff, A.; Sehested, J.; Chorkendorff, I.; Helveg, S.; Nielsen, J. H. *J. Phys. Chem. C* **2015**, *119*, 2804–2812.

(23) Tao, F.; Grass, M. E.; Zhang, Y.; Butcher, D. R.; Renzas, J. R.; Liu, Z.; Chung, J. Y.; Mun, B. S.; Salmeron, M.; Somorjai, G. A. *Science* **2008**, *322*, 932–934.

(24) Ahmadi, M.; Behafarid, F.; Cui, C.; Strasser, P.; Cuenya, B. R. *ACS Nano* **2013**, *7*, 9195–9204.

(25) Carenco, S.; Wu, C. H.; Shavorskiy, A.; Alayoglu, S.; Somorjai, G. A.; Bluhm, H.; Salmeron, M. *Small* **2015**, *11*, 3045–3053.

(26) Hodak, J. H.; Henglein, A.; Giersig, M.; Hartland, G. V. *J. Phys. Chem. B* **2000**, *104*, 11708–11718.

(27) Liao, H.; Fisher, A.; Xu, Z. J. *Small* **2015**, *11*, 3221–3246.

(28) Sarkar, R.; Rentenberger, C.; Rajagopalan, J. *Sci. Rep.* **2015**, *5*, 1–11.

(29) Woehl, T. J.; Evans, J. E.; Arslan, I.; Ristenpart, W. D.; Browning, N. D. *ACS Nano* **2012**, *6*, 8599–8610.

(30) Van Den Berg, R.; Elkjaer, C. F.; Gommes, C. J.; Chorkendorff, I.; Sehested, J.; De Jongh, P. E.; De Jong, K. P.; Helveg, S. *J. Am. Chem. Soc.* **2016**, *138*, 3433–3442.

(31) Gorelikov, I.; Matsuura, N. *Nano Lett.* **2008**, *8*, 369–373.

(32) Guisbiers, G.; Mendoza-Cruz, R.; Bazán-Díaz, L.; Velázquez-Salazar, J. J.; Mendoza-Perez, R.; Robledo-Torres, J. A.; Rodriguez-Lopez, J. L.; Montejano-Carrizales, J. M.; Whetten, R. L.; José-Yacamán, M. *ACS Nano* **2016**, *10*, 188–198.

(33) Mallard, W.; Gardner, A. B.; Bass, R.; Slifkin, L. *Phys. Rev.* **1963**, *129*, 617–625.

(34) Doyama, M.; Koehler, J. S. *Phys. Rev.* **1962**, *127*, 21–31.

(35) Simmons, R. O.; Balluffi, R. W. *Phys. Rev.* **1962**, *125*, 862–872.

(36) Hagel, W.; Westbrook, J. *Trans. TMS-AIME* **1961**, *221*, 951.

(37) Mortlocks, A. J.; Tomlm, D. H. *Philo. Mag.* **1959**, *4*, 628–643.

(38) Peart, R.; Tomlin, D. *Acta Metall.* **1962**, *10*, 123 – 134.

(39) Resing, H.; Nachtmeb, N. *J. Phys. Chem. Sol.* **1962**, *21*, 40 – 56.

(40) Guisbiers, G.; Buchaillot, L. *J. Phys. Chem. C* **2009**, *113*, 3566–3568.

(41) Guisbiers, G. *Nanoscale Res. Lett.* **2010**, *5*, 1132–1136.

(42) Ye, X.; Zheng, C.; Chen, J.; Gao, Y.; Murray, C. B. *Nano Lett.* **2013**, *13*, 765–â“771.

(43) Ravel, B.; Newville, M. *Journal of Synchrotron Radiation* **2005**, *12*, 537–541.